

## Photoionization from $1sns\ ^{1,3}S^e$ states of helium

T. N. Chang

*Department of Physics, University of Southern California, Los Angeles, California 90089-0484*

M. Zhen

*Department of Physics, Fujian Teachers University, Fuzhou, Fujian, People's Republic of China*

(Received 11 January 1993)

We present theoretical photoionization cross sections from the  $1sns\ ^{1,3}S^e$  bound excited states of the helium atom based on a configuration-interaction procedure for the *continuum*, using a finite  $L^2$ -basis set constructed from a nearly complete set of  $B$ -spline-based one-particle hydrogenic orbitals. In addition to the nonresonant spectra near the first ionization threshold, resonant structures associated with selected  $sp, 2n^\pm$  and  $2pnd\ ^{1,3}P^o$  autoionization series below the  $\text{He}^+ N=2$  threshold are examined in detail. The widths and resonance energies of all  $^{1,3}P$  autoionization series are also reported and compared with other available theoretical and experimental results.

PACS number(s): 32.80.Fb, 32.80.Dz, 31.20.Tz, 32.70.Jz

### I. INTRODUCTION

The *absolute* photoionization cross sections of excited He atoms were first measured by Stebbings *et al.* [1] in the nonresonant region from the ionization threshold to 2400 Å. Specifically, the  $\text{He}^+$  ions were measured following the application of a frequency-doubled tunable dye laser to a beam of  $\text{He}\ 1s2s\ ^{1,3}S^e$  metastable atoms, which was irradiated with a helium discharge lamp after electron-impact excitation of a He atom from its ground state. For nearly 20 years, lack of a high-resolution intense light source in the shorter-wavelength region (i.e.,  $\sim 325$  Å or shorter) has limited the extension of such measurement to the resonant region dominated by autoionization states with widths of, typically, 10 meV or less. Since the peak photoionization cross sections to doubly excited resonances from the  $1s2s\ ^{1,3}S^e$  metastable states can be several orders of magnitude greater than the cross sections from the ground state, recent development in high-resolution monochromator operating with high synchrotron radiation intensity [2] may have opened up the experimental possibility to the resonant region if high-density metastable He atoms can be generated.

Theoretically, by using an asymptotically correct continuum wave function with a phase shift extrapolated from quantum defects, Burgess and Seaton [3] have derived a general formula for the nonresonant photoionization. Burgess and Seaton's approach is physically more realistic than the ones that use pure Coulomb continuum wave functions (e.g., in earlier works by Huang [4] and Goldberg [5]). As a result, the predicted near-threshold photoionization cross sections from  $\text{He}\ 1s2s\ ^{1,3}S$  states by Burgess and Seaton agree well with the measured absolute cross sections by Stebbings *et al.* [1]. In fact, for the  $1s2s\ ^3S$  photoionization, the result of Burgess and Seaton actually agrees better with the observed spectrum than the subsequent  $1s2s2p$  close-coupling result by Norcross [6]. A more comprehensive calculation, with a close-

coupling final-state continuum function and a Hylleraas-type correlated initial-state wave function, was carried out by Jacobs [7] for photon energy up to the lowest doubly excited autoionization state. Similar to the earlier results of Burgess and Seaton, the calculated  $\text{He}\ 1s2s\ ^1S$  near-threshold photoionization cross sections by Jacobs agree very well with the observed spectra by Stebbings *et al.* [1]. A bound-state expansion method has also been developed and applied by Dalgarno and co-workers [8] to the  $\text{He}\ 1s2s\ ^{1,3}S$  photoionization from the ionization threshold up to the lowest doubly excited  $sp, 22^{+1,3}P$  resonances. Their calculated nonresonant  $1s2s\ ^1S$  photoionization cross sections agree well with the close-coupling results by Jacobs [7]. As for the nonresonant  $1s2s\ ^3S$  photoionization, the calculated cross sections by Dalgarno and co-workers are in agreement with the results of Burgess and Seaton [3], which are slightly below the experimental values near the ionization threshold but within the experimental uncertainties. The theoretical widths of the doubly excited resonances from the  $1s2s2p$  close-coupling calculations [6,7] are, in general, noticeably different from the more accurate theoretical results that use either a more extended close-coupling calculation [9] or a more elaborate complex-rotational method [10]. The calculated width by Dalgarno and co-workers [8] agrees well with other more elaborate calculations for the  $sp, 22^{+1}P$  resonance but not the  $sp, 22^{+3}P$  resonance.

The main purpose of this paper is to present the result of a more comprehensive photoionization calculation for He atoms from the  $1sns\ ^{1,3}S^e$  bound excited states at energies ranging from the ionization threshold to the spectral region dominated by the  $sp, 2n^\pm$  and  $2pnd\ ^{1,3}P^o$  autoionization series. The accuracy of our final-state continuum wave functions is demonstrated by the close agreement between the present calculation and other most accurate theoretical calculations in terms of (i) the  $e\text{-He}^+\ ^{1,3}P$  scattering phase shifts in the nonresonant region and (ii) the resonant widths of the doubly excited au-

toionization states in the resonant region. Our calculation is carried out based on a configuration-interaction procedure for the *continuum* (CIC) [11], which has been applied successfully to the photoionization of the two-electron atom and the single- and multiphoton ionization of the divalent atom. By expanding the size of the basis set, the energy and width of the doubly excited autoionization states can be determined more accurately by examining the energy variation of the probability density corresponding to the ionization channel following a more elaborate *B*-spline-based configuration-interaction procedure [12].

In Sec. II, we present our nonresonant photoionization cross sections from He  $1s2s\ ^1,^3S^e$  metastable states and other higher  $1sns\ ^1,^3S^e$  excited states. We also compare the nonresonant  $e\text{-He}^+{}^{1,3}P$  scattering phase shifts between the present calculation and the most accurate 20-state close-coupling calculation by Oza [9]. In Sec. III, we present the photoionization spectra dominated by the  $sp, 2n^\pm$  and  $2pnd\ ^1,^3P^o$  autoionization series. Our calculated resonant energy and width of the doubly excited autoionization series are also compared with the most accurate existing theoretical results.

## II. NONRESONANT PHOTOIONIZATION

By using a *B*-spline-based CIC procedure outlined elsewhere [11,13], the effect due to electron-electron correla-

tion is included in the state wave functions of both initial and final states of the photoionization. Figure 1 presents the variation of nonresonant  $e\text{-He}^+{}^{1,3}P$  scattering phase shifts as the size of the basis set of the CIC calculation is increased from a single  $1sp$  configuration series to a total of 89 series. Clearly, the phase shifts from the single-ionization channel calculation, which are represented by the solid curves labeled as  $1sp$  series only, differ significantly from our final results. The corrections in phase shift due to the addition of  $2sp, 2ps,$  and  $2pd$  series to the  $1sp$  series account for nearly half of the phase-shift difference. Our calculated phase shifts, including only the  $1sp, 2sp, 2ps,$  and  $2pd$  series in the basis set, agree well with the  $1s2s2p$  close-coupling results of Norcross [6], as shown. Between 30–40% and approximately 25% of the phase-shift difference can be attributed to the  $npd$  type of configuration series for the  $^1P$  and  $^3P$  continua, respectively. Our converged phase shifts are in excellent agreement with the 20-state close-coupling results by Oza [9]. Also, the phase shifts at zero energy approach the expected values  $\pi\mu$  (where  $\mu$  is the quantum defect), which equal  $-0.038$  and  $0.214$  for the  $^1P$  and  $^3P$  series, respectively. All two-electron configuration functions included in the basis set of the nonresonant photoionization calculations are of the bound-bound or bound-continuum type [14], i.e., each of the two-electron basis functions in the CIC calculation consists of at least one negative-energy single-particle orbital function. We have tested and

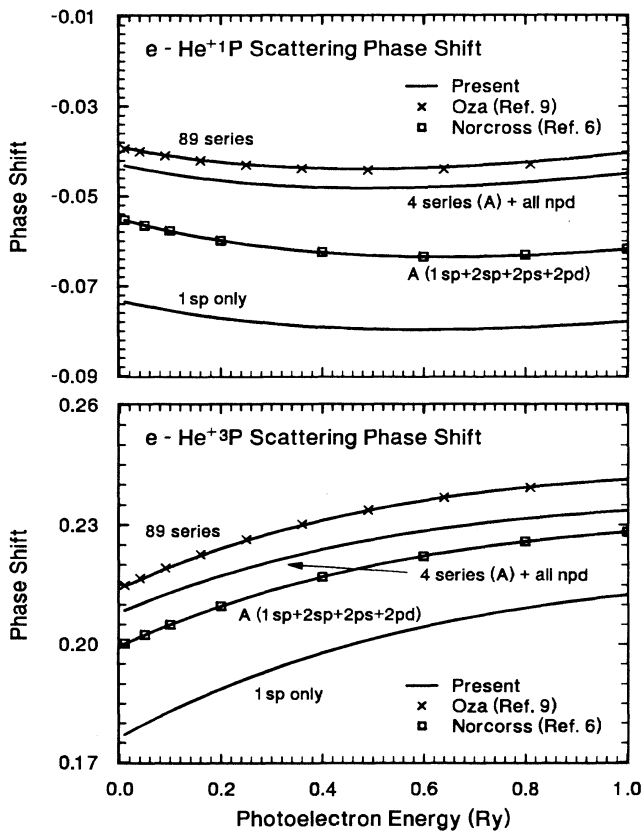


FIG. 1. Variation of nonresonant  $e\text{-He}^+{}^{1,3}P$  scattering phase shifts as functions of photoelectron energy.

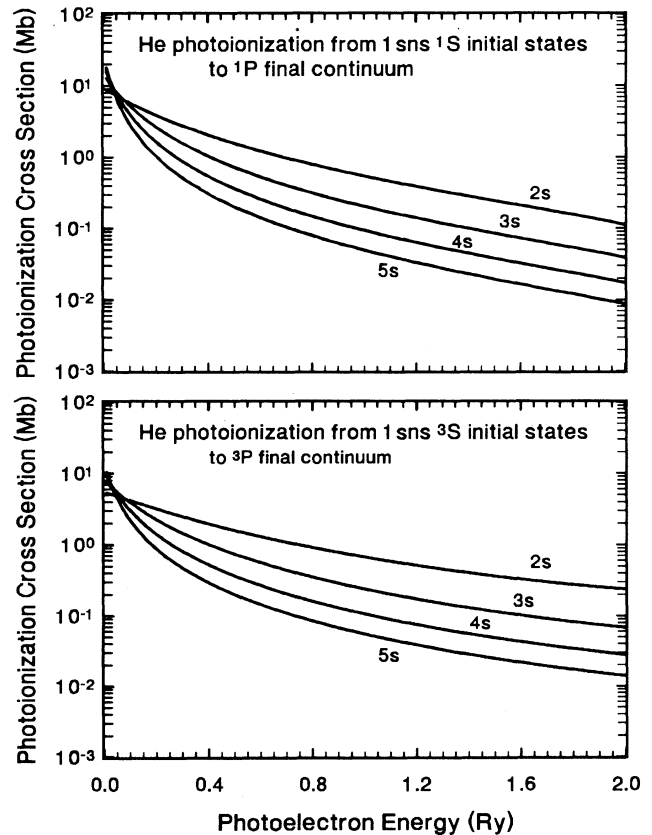


FIG. 2. Nonresonant photoionization cross sections from He  $1sns\ ^1,^3S$  bound excited states.

TABLE I. The nonresonant photoionization cross sections (in Mb) from He  $1s2s\ 1,3S$  metastable states. The photoelectron energy  $\epsilon$  is given in Ry. Only length results are listed.

$\epsilon$ (Ry)	$1s2s\ 1S$			$1s2s\ 3S$		
	Present	$A^a$	$B^b$	Present	$A^a$	$B^b$
0.01	8.798	8.753	9.350	5.345		4.751
0.05	7.258	7.128	7.083	4.804		4.332
0.10	5.803	5.671	5.413	4.188		4.042
0.15	4.722	4.473		3.654	3.537	
0.20	3.902	3.821	3.904	3.199	3.157	3.509
0.25	3.268	3.233		2.812	2.796	
0.30	2.770	2.768		2.485	2.480	
0.40	2.047	2.068	2.122	1.968	1.970	1.993
0.60	1.225	1.233	1.258	1.302	1.311	1.268
0.80	0.795	0.794	0.858	0.913	0.926	0.918
1.00	0.546	0.543	0.490	0.671	0.685	0.629
1.20	0.390	0.388	0.319	0.512	0.527	0.500
1.40	0.285	0.284	0.277	0.404	0.418	0.449
1.60	0.212	0.211	0.219	0.328	0.342	0.372

<sup>a</sup>Jacobs [7].

<sup>b</sup>Norcross [6].

found that the contribution from the continuum-continuum type of two-electron functions to the scattering phase shift in the nonresonant region is negligible.

The nonresonant photoionization cross sections from He  $1sns\ 1,3S^e$  excited states are shown in Fig. 2. The overall agreement between our length and velocity results is about 1% or better, and only the length results are shown. In Table I, our theoretical photoionization cross sections at selected photoelectron energies are compared with the close-coupling results of Jacobs [7] and Norcross [6]. At energies immediately next to the threshold, our theoretical results differ noticeably from the close-coupling calculation by Norcross [6], which employed an essentially uncorrelated initial-state wave function. Our

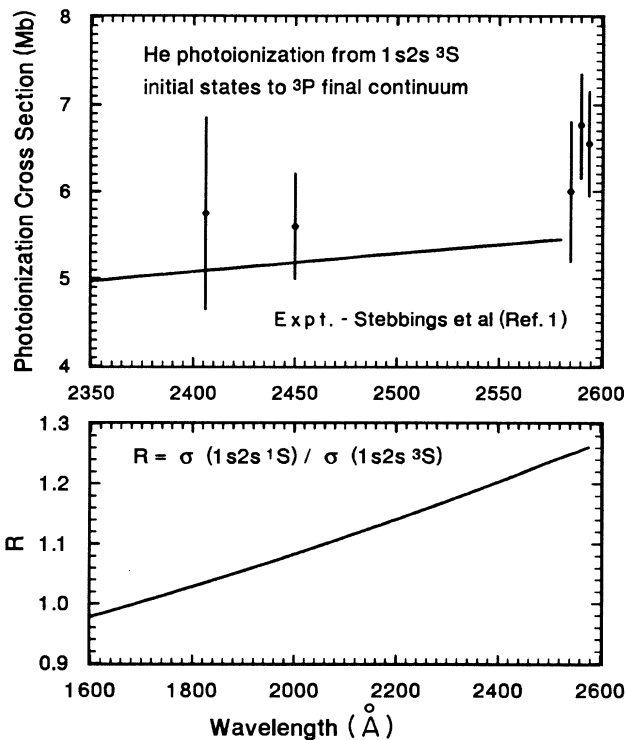


FIG. 3. Near-threshold photoionization cross sections from He  $1s2s\ 3S$  metastable state and the ratio  $R$  between the  $1s2s\ 1S$  and  $1s2s\ 3S$  photoionization cross sections.

nonresonant photoionization cross sections from other  $1sns\ 1,3S$  bound excited states are listed in Table II.

For the  $1s2s\ 1S^e \rightarrow 1P^o$  photoionization, most of the theoretical cross sections, including the present results and those by Burgess and Seaton [3], Jacobs [7], and Dalgarno and co-workers [8], are in close agreement with each other, and they also agree well with the observed

TABLE II. The nonresonant photoionization cross sections (in Mb) from He  $1sns\ 1,3S$  bound excited states with  $n = 3-5$ . The photoelectron energy  $\epsilon$  is given in Ry. Only length results are listed.

$\epsilon$ (Ry)	$1sns\ 1S$			$1sns\ 3S$		
	3s	4s	5s	3s	4s	5s
0.01	12.77	16.06	18.14	7.409	9.118	10.28
0.05	8.256	7.754	6.525	5.466	5.172	4.391
0.10	5.287	4.039	2.891	3.908	3.025	2.177
0.15	3.656	2.463	1.629	2.918	1.986	1.311
0.20	2.669	1.654	1.043	2.256	1.406	0.880
0.25	2.026	1.182	0.712	1.792	1.047	0.627
0.30	1.586	0.884	0.522	1.455	0.810	0.472
0.40	1.040	0.544	0.309	1.011	0.524	0.294
0.50	0.728	0.365	0.203	0.739	0.366	0.200
0.60	0.534	0.260	0.142	0.562	0.268	0.145
0.70	0.405	0.193	0.105	0.440	0.205	0.109
0.80	0.316	0.148	0.0794	0.353	0.161	0.0848
0.90	0.252	0.116	0.0616	0.289	0.129	0.0675
1.00	0.204	0.0934	0.0492	0.240	0.106	0.0550
1.20	0.140	0.0630	0.0327	0.173	0.0748	0.0383
1.40	0.0995	0.0444	0.0229	0.130	0.0553	0.0282
1.60	0.0725	0.0321	0.0165	0.101	0.0425	0.0216

data near the ionization threshold [1]. For the  $1s2s\ ^3S^e \rightarrow\ ^3P^o$  photoionization, the present results also agree well with the existing theoretical results [3,7,8]. Similar to the earlier results of Burgess and Seaton [3], our near-threshold  $1s2s\ ^3S^e \rightarrow\ ^3P^o$  cross sections shown in Fig. 3 appear to be slightly less than the observed values but clearly within the experimental error bars. The ratio  $R$  between the  $1s2s\ ^1S$  and  $1s2s\ ^3S$  cross sections as a function of wavelength is also shown in Fig. 3. The ratio  $R$  appears to deviate significantly from unity, especially at shorter wavelengths. As a result, we could not confirm the experimental observation that the  $1s2s\ ^1S$  cross section nearly equals the  $1s2s\ ^3S$  cross section at energies close to the ionization threshold [1].

### III. DOUBLY EXCITED RESONANCES

In Fig. 4, we present our calculated photoionization spectra from He  $1s2s\ ^{1,3}S^e$  metastable states to the resonant region dominated by the  $^{1,3}P^o$  doubly excited resonances. Similar to the  $^1P$  photoionization spectra from the  $1s^2\ ^1S$  ground state [2,13], the  $sp, 2(n+1)^-$  and  $2pnd\ ^1P$  resonances are separated by approximately 16 meV and 9 meV for the  $n=3$  and 4 pairs, respectively. Except for the  $sp, 2n^+\ ^{1,3}P$  series, the peak cross sections  $\sigma_{\max}$  for the narrower  $sp, 2n^-$  and  $2pnd\ ^{1,3}P$  states are

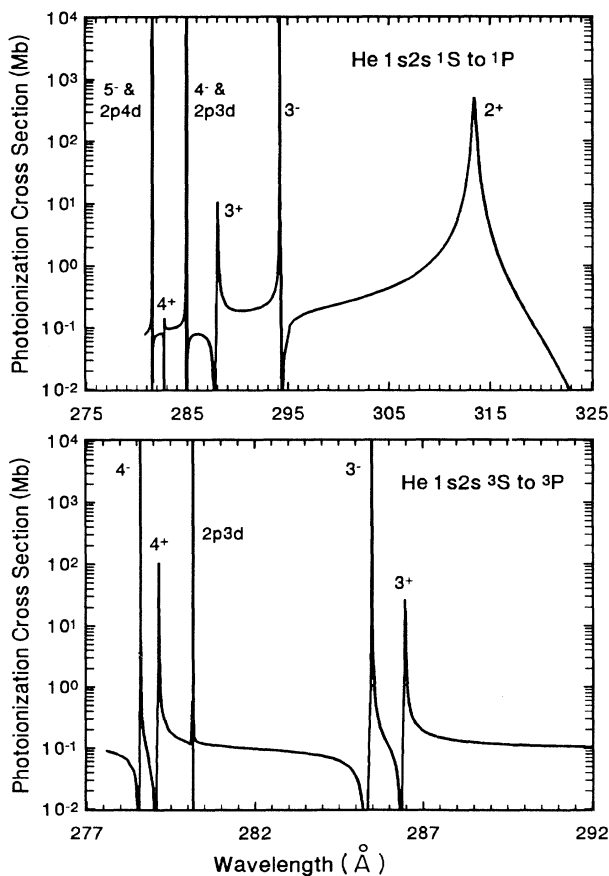


FIG. 4. Photoionization spectra from He  $1s2s\ ^{1,3}S$  metastable states to  $^{1,3}P$  doubly excited resonances.

significantly larger than the nonresonant photoionization cross sections. Detailed photoionization structures as functions of photoelectron energy from  $1sns\ ^{1,3}S$  excited states to a few selected doubly excited states are given in Figs. 5 and 6 for the  $^1P$  and  $^3P$  resonances, respectively. The spectra shown in Figs. 4–6 are obtained from a CIC calculation with a total of 23 configuration series, which includes only bound-bound and bound-continuum types of two-electron configuration functions. Our calculated oscillator strength values, i.e.,  $f_{EI}$  in Eq. (20) of the first Ref. [11], are essentially converged, and the length and velocity results agree very well with each other.

For an *isolated* autoionization state of resonant energy  $E_r$ , its resonant structure is best described by the Fano formula [15] in terms of a set of resonant parameters, which include the resonant width  $\Gamma$ , the asymmetry parameter  $q$ , and the nonresonant background cross section  $\sigma_b$ . The peak cross section  $\sigma_{\max}$ , located at  $E_{\max} = E_r + \frac{1}{2}(\Gamma/q)$  according to the Fano formula, equals  $\sigma_b(1+q^2)$ . Also, the cross section is expected to reach a zero at an energy  $E_{\min} = E_r - \frac{1}{2}(\Gamma/q)$ . For photoionization from bound excited states, the  $q$  value is often significantly larger than the one for transition from the ground state, i.e., a nearly symmetric resonant profile is usually observed with  $E_{\max} \approx E_r$ , and the zero in the cross section is located far away from the center of the resonance. For multiple series of closely situated autoionization structures, the zero cross section may no longer be present at all due to the interference between neighboring resonances, and the  $q$  parameter becomes less effective in characterizing the resonance profile.

Alternatively, the autoionization structures can be described quantitatively in terms of their  $E_r$ ,  $\Gamma$ , and  $\sigma_{\max}$ . In the present calculation, more accurate values of the energy and width of the doubly excited autoionization state are determined by examining the energy variation of the probability density of the ionization channel with a substantially enlarged basis set that includes configuration functions of the bound-bound, bound-continuum, and continuum-continuum types. The calculational procedure of this more elaborate  $B$ -spline-based configuration-interaction (CI) method is given in detail elsewhere [12]. In Tables III and IV, we list our calculated widths and energies of all doubly excited  $^{1,3}P$  series below the He<sup>+</sup>  $N=2$  threshold. Our resonant energies appear to compare very well with some of the most accurate theoretical calculations. The agreement in resonant widths between different theories is generally good for the broader states. For the narrow states, the resonant widths differ significantly. For the “+” and “-” series, the theoretical widths from the 23-series CI calculation (not shown in Tables III and IV) are generally greater than the listed widths, which include additional contributions from the continuum-continuum type of configuration series in the enlarged CI calculation. The resonant energies from the  $1s2s2p$  close-coupling calculation by Norcross [6], listed in Tables III and IV, are converted from the wavelengths using  $R(^4\text{He}) = 109\,722.273\,09\ \text{cm}^{-1}$ , and the term values of  $32\,033.321\ \text{cm}^{-1}$  and  $38\,454.8295\ \text{cm}^{-1}$  for the  $1s2s\ ^1S$  and  $1s2s\ ^3S$  states, respectively [20]. For the  $^1P$  series,

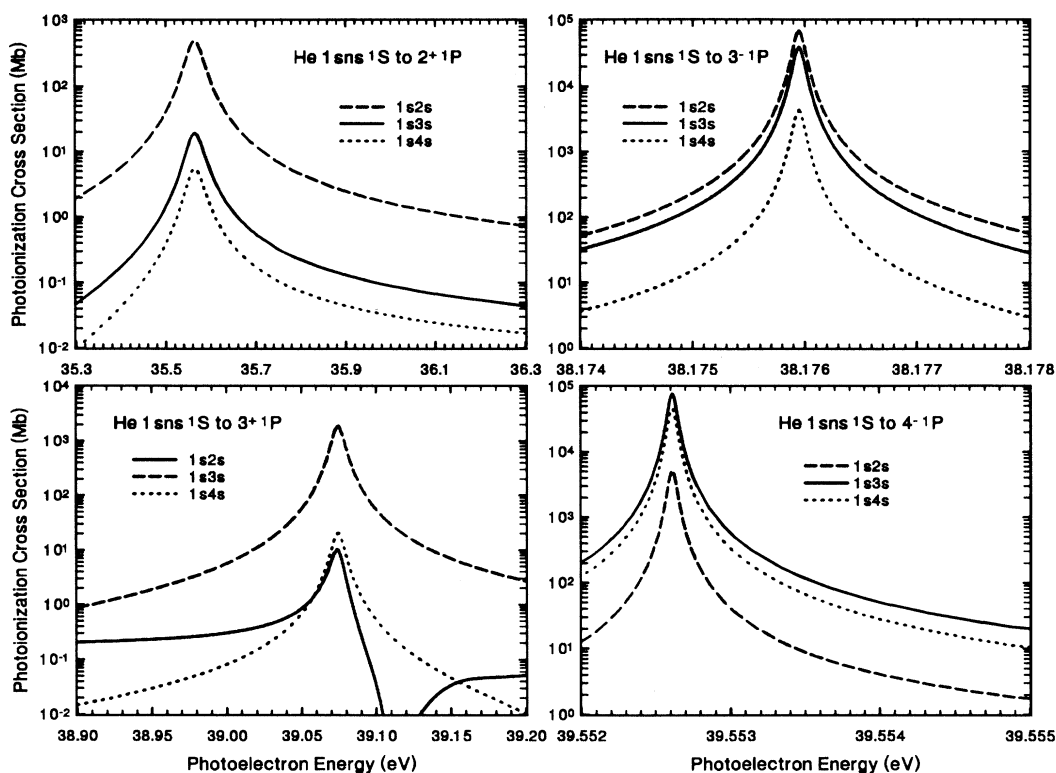


FIG. 5. Photoionization spectra from  $1sns\ 1S$  bound excited states to selected doubly excited  $1P$  autoionization states.

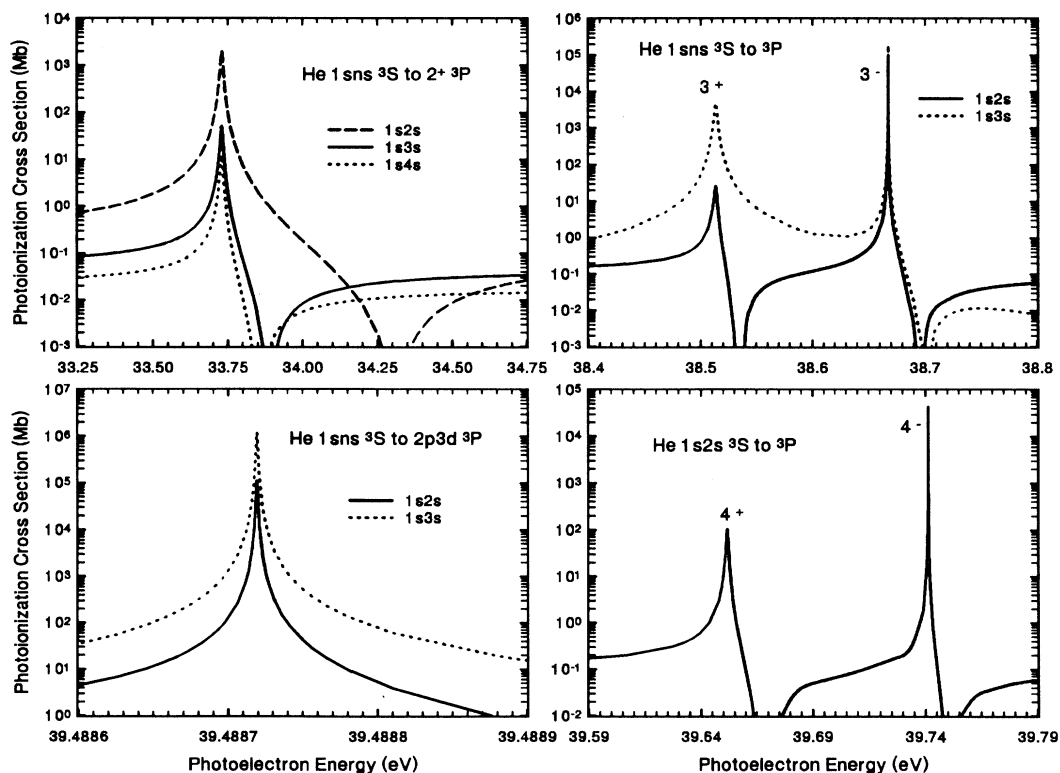


FIG. 6. Photoionization spectra from  $1sns\ 3S$  bound excited states to selected doubly excited  $3P$  autoionization states.

TABLE III. The resonant energies (upper entry, in Ry) and widths (lower entry, in the format  $a[-b]=a \times 10^{-b}$  Ry) of selected He  $sp, 2n^{\pm}$  and  $2pd$   $^1P$  resonances below the  $N=2$  threshold.

State	Present	$A^a$	$B^b$	$C^c$	$D^d$	$E^e$	$F^f$
$2^+$	-1.386 103 2.78[-3]	-1.3856 2.66[-3]	-1.386 270 2.75[-3]	-1.385 50 2.69[-3]	-1.384 26 2.75[-3]	-1.3859 2.70[-3]	-1.377 36 3.22[-3]
$3^+$	-1.128 108 6.08[-4]	-1.128 02 6.2[-4]	-1.128 170 6.02[-4]	-1.127 674 6.20[-4]	-1.127 58 6.21[-4]		-1.125 86 6.41[-4]
$4^+$	-1.068 701 2.60[-4]	-1.068 643 2.48[-4]	-1.068 722 2.58[-4]	-1.068 374 2.67[-4]	-1.068 50 2.66[-4]		-1.067 72 2.71[-4]
$5^+$	-1.042 995 1.34[-4]	-1.042 978 1.32[-4]	-1.043 000 1.29[-4]				
$3^-$	-1.194 147 7.67[-6]	-1.194 145 7.78[-6]	-1.194 148 7.70[-6]	-1.194 106 6.95[-6]	-1.194 60 1.05[-5]	-1.1943 8.53[-6]	-1.193 35 1.03[-5]
$4^-$	-1.092 965 4.00[-6]	-1.092 951 4.16[-6]	-1.092 987 4.10[-6]	-1.092 918 4.40[-6]	-1.092 260 1.54[-6]		-1.093 19 3.71[-6]
$5^-$	-1.054 585 1.95[-6]	-1.054 578 2.04[-6]	-1.054 590				
$3d$	-1.094 141 5 ~2.4[-7]	-1.093 85	-1.094 185 3.2[-8]	-1.093 736 3.1[-9]	-1.094 020 2.23[-6]		-1.090 49 1.13[-7]
$4d$	-1.055 207 2 ~7.1[-8]		-1.055 221	-1.055 092 7.86[-8]	-1.055 10 9.41[-7]		

<sup>a</sup>Oza [9].

<sup>b</sup>Ho [10].

<sup>c</sup>Wu and Xi [16].

<sup>d</sup>Macias and Riera [17].

<sup>e</sup>Tang, Watanabe, and Matsuzawa [18].

<sup>f</sup>Norcross [6].

comparison with a few other recent theoretical results [21–24] can also be found elsewhere [13].

Unlike the resonant widths, our calculated oscillator strengths are not affected noticeably by the addition of the continuum-continuum type of configuration series in

the basis set of the CI calculation. Since  $\sigma_{\max}$  is inversely proportional to  $\Gamma$  (see, e.g., Eq. (46) of Ref. [25]), the correct  $\sigma_{\max}$  should be greater than those appear in Figs. 4–6 as the widths of the resonances are reduced and the oscillator strengths remain unchanged. The modified

TABLE IV. The resonant energies (upper entry, in Ry) and widths (lower entry, in the format  $a[-b]=a \times 10^{-b}$  Ry) of selected He  $sp, 2n^{\pm}$  and  $2pd$   $^3P$  resonances below the  $N=2$  threshold.

State	Present	$A^a$	$B^b$	$C^c$	$D^d$	$E^e$	$F^f$
$2^+$	-1.520 949 5.80[-4]	-1.520 902 6.02[-4]	-1.520 985 5.98[-4]	-1.521 712 7.72[-4]	-1.521 224 6.01[-4]	-1.5210 5.98[-4]	-1.517 69 7.81[-4]
$3^+$	-1.169 334 1.58[-4]	-1.169 304 1.54[-4]	-1.169 345 1.65[-4]	-1.169 524 1.37[-4]	-1.169 437 1.68[-4]		-1.166 24 2.28[-4]
$4^+$	-1.085 676 6.20[-5]	-1.085 660 6.04[-5]	-1.085 675 6.24[-5]	-1.085 624 7.64[-5]	-1.085 910 6.08[-5]		-1.084 31 9.04[-5]
$5^+$	-1.051 422 2.95[-5]	-1.051 417 2.88[-5]	-1.051 42 2.76[-5]	-1.049 496 3.30[-5]			
$3^-$	-1.158 055 3.95[-6]	-1.158 049 3.56[-6]	-1.158 062 3.78[-6]	-1.157 992 3.98[-6]	-1.158 330 4.12[-6]	-1.1583 3.54[-6]	-1.156 31 5.66[-6]
$4^-$	-1.079 115 1.67[-6]		-1.079 118 1.54[-6]	-1.079 002 8.89[-6]	-1.079 412 9.6[-7]		-1.078 56 2.31[-5]
$3d$	-1.097 661 ~6[-7]	-1.097 594 8 2.18[-8]	-1.097 689 2[-8]	-1.097 504 7.6[-8]	-1.097 774 1.84[-8]		-1.094 22 3.32[-7]
$4d$	-1.057 263 ~2.7[-7]		-1.057 277	-1.056 018 4.8[-7]	-1.057 411 1.26[-8]		

<sup>a</sup>Oza [9].

<sup>b</sup>Ho [10], and private communication.

<sup>c</sup>Wu and Xi [16].

<sup>d</sup>Moccia and Spizzo [19].

<sup>e</sup>Tang, Watanabe, and Matsuzawa [18].

<sup>f</sup>Norcross [6].

TABLE V. The peak photoionization cross section  $\sigma_{\max}$  (in the format  $a[b]=a \times 10^b$  Mb) from selected  $1sns\ 1,3S$  bound excited states to  $sp, 2n^\pm$  and  $2pnd\ 1,3P$  resonances below the  $N=2$  threshold of  $\text{He}^+$ .

Bound excited state	$\sigma_{\max}$					
	$sp, 22^+$	$sp, 23^+$	$sp, 24^+$	$sp, 23^-$	$sp, 24^-$	$2p3d$
	$^1P$ resonances					
$1s2s\ ^1S$	5.193[2]	1.079[1]	1.513[-1]	7.518[4]	6.257[3]	2.495[5]
	4.36[2] <sup>a</sup>	1.52[1] <sup>a</sup>	2.06[0] <sup>a</sup>	6.55[4] <sup>a</sup>	2.87[4] <sup>a</sup>	4.79[4] <sup>a</sup>
$1s3s\ ^1S$	2.029[1]	1.968[3]	4.281[1]	4.217[4]	9.271[4]	2.093[5]
$1s4s\ ^1S$	5.844[0]	2.148[1]	4.588[3]	4.618[3]	5.537[4]	4.715[5]
	$^3P$ resonances					
$1s2s\ ^3S$	2.554[3]	3.255[1]	1.274[2]	8.059[4]	4.328[4]	1.625[4]
	1.99[3] <sup>a</sup>	3.78[0] <sup>a</sup>	4.53[1] <sup>a</sup>	5.54[4] <sup>a</sup>	3.17[4] <sup>a</sup>	4.07[4] <sup>a</sup>
$1s3s\ ^3S$	6.183[1]	6.244[3]	4.094[2]	1.922[5]	4.524[4]	1.816[5]
$1s4s\ ^3S$	1.510[1]	2.033[2]	1.376[4]	3.983[3]	5.273[5]	4.032[4]

<sup>a</sup>Norcross [6].

$\sigma_{\max}$  for selected transitions, after taking into account the reduction in  $\Gamma$ , are listed in Table V. Similar to our non-resonant calculation, the agreement between our length and velocity results is better than 1%. Only the length results are included in Table V. The  $1s2s2p$  close-coupling results by Norcross [6] for the  $1s2s\ 1,3S \rightarrow 1,3P$  transitions are also listed for comparison. For the  $1s2s\ ^1S \rightarrow sp, 22^+ ^1P$  transition, our theoretical  $\sigma_{\max} = 519.3$  Mb is in agreement with the calculated value of 541 Mb by Dalgarno and co-workers [8], but differs noticeably from the close-coupling results of 436 Mb and 384 Mb by Norcross [6] and Jacobs [7], respectively. This disagreement may be partially attributed to the approximately 15% overestimation in width from the close-coupling calculations in comparison with most of the existing theoretical values shown in Table III. For the  $1s2s\ ^3S \rightarrow sp, 22^+ ^3P$  transition, our theoretical  $\sigma_{\max} = 2554$  Mb is greater than the results from all three previous calculations [6–8]. This discrepancy can be attributed *entirely* to the difference in the calculated resonant widths. In fact, the  $\sigma_{\max}$  would range from 2400 to

2500 Mb for these three calculations if adjustment due to the difference in resonant width is taken into account.

In contrast to the strongly asymmetric ground-state spectrum, the presence of more symmetric resonant profiles in bound excited-state spectra suggests that, experimentally, both  $\Gamma$  and  $E_r$  of a doubly excited autoionization state can also be determined, perhaps less ambiguously, from photoionization of bound excited states. Recent development of a more intense light source in a more extended spectral region should also help in leading to the observation of high-resolution photoionization spectra dominated by the doubly excited resonances from bound excited states, at least for those resonances with high peak cross sections.

#### ACKNOWLEDGMENTS

This work was supported by NSF under Grant No. PHY91-11420. One of us (MZ) would like to acknowledge the support from the Ministry of Education of People's Republic of China.

- [1] R. F. Stebbings, F. B. Dunning, F. K. Tittel, and R. D. Rundel, *Phys. Rev. Lett.* **30**, 815 (1973).
- [2] M. Domke, G. Remmers, and G. Kaindl, *Phys. Rev. Lett.* **69**, 1171 (1992).
- [3] A. Burgess and M. J. Seaton, *Mon. Not. R. Astron. Soc.* **120**, 121 (1960).
- [4] S. S. Huang, *Astrophys. J.* **108**, 354 (1948).
- [5] L. Goldberg, *Astrophys. J.* **90**, 414 (1939).
- [6] D. W. Norcross, *J. Phys. B* **4**, 652 (1971).
- [7] V. L. Jacobs, *Phys. Rev. A* **3**, 289 (1971); **4**, 939 (1971); **9**, 1938 (1974).
- [8] A. Dalgarno, H. Doyle, and M. Oppenheimer, *Phys. Rev. Lett.* **29**, 1051 (1972); H. Doyle, M. Oppenheimer, and A. Dalgarno, *Phys. Rev. A* **11**, 909 (1975).
- [9] D. H. Oza, *Phys. Rev. A* **33**, 824 (1986).
- [10] Y. K. Ho, *Z. Phys. D* **21**, 191 (1991); *Phys. Rev. A* **34**, 4402 (1986).
- [11] T. N. Chang and X. Tang, *Phys. Rev. A* **44**, 232 (1991); **46**, 2209 (1992).
- [12] T. N. Chang, *Phys. Rev. A* **47**, 705 (1993).
- [13] T. N. Chang, *Phys. Rev. A* **47**, 3441 (1993).
- [14] T. N. Chang and R. Q. Wang, *Phys. Rev. A* **43**, 1218 (1991).
- [15] U. Fano, *Phys. Rev.* **124**, 1866 (1961).
- [16] L. Wu and J. Xi, *J. Phys. B* **23**, 727 (1990).
- [17] A. Macias and A. Riera, *Europhys. Lett.* **2**, 351 (1986); *Phys. Lett. A* **119**, 28 (1986).
- [18] J. Tang, S. Watanabe, and M. Matsuzawa, *Phys. Rev. A* **46**, 2437 (1992).
- [19] R. Moccia and P. Spizzo, *J. Phys. B* **20**, 1423 (1987).
- [20] A. Kono and S. Hattori, *Phys. Rev. A* **34**, 1727 (1986).
- [21] S. Salomonson, S. L. Carter, and H. P. Kelly, *Phys. Rev. A* **39**, 5111 (1989).
- [22] R. Gersbacher and T. Broad, *J. Phys. B* **23**, 365 (1990).
- [23] I. Sánchez and F. Martín, *J. Phys. B* **23**, 4263 (1990).
- [24] P. Hamacher and J. Hinz, *J. Phys. B* **22**, 3397 (1989).
- [25] T. N. Chang, *Phys. Rev. A* **37**, 4090 (1988).